Astron. Astrophys. 362, 419–425 (2000)

ASTRONOMY AND ASTROPHYSICS

Type Ia supernova rate at $z \sim 0.1^{\star}$

The EROS collaboration

D. Hardin[1,⋆⋆], C. Afonso[1], C. Alard[9], J.N. Albert[2], A. Amadon[1], J. Andersen[6], R. Ansari[2], É. Aubourg[1], P. Bareyre[1,4], F. Bauer[1], J.P. Beaulieu[5], G. Blanc[1], A. Bouquet[4], S. Char[7], X. Charlot[1], F. Couchot[2], C. Coutures[1], F. Derue[2], R. Ferlet[5], J.F. Glicenstein[1], B. Goldman[1], A. Gould[1,8], D. Graff[8], M. Gros[1], J. Haissinski[2], J.C. Hamilton[4], J. de Kat[1], A. Kim[4], T. Lasserre[1], É. Lesquoy[1], C. Loup[5], C. Magneville[1], B. Mansoux[2], J.B. Marquette[5], É. Maurice[3], A. Milsztajn[1], M. Moniez[2], N. Palanque-Delabrouille[1], O. Perdereau[2], L. Prévot[3], N. Regnault[2], J. Rich[1], M. Spiro[1], A. Vidal-Madjar[5], L. Vigroux[1], and S. Zylberajch[1]

[1] CEA, DSM, DAPNIA, Centre d'Études de Saclay, 91191 Gif-sur-Yvette Cedex, France
[2] Laboratoire de l'Accélérateur Linéaire, IN2P3 CNRS, Université de Paris-Sud, 91405 Orsay Cedex, France
[3] Observatoire de Marseille, 2 pl. Le Verrier, 13248 Marseille Cedex 04, France
[4] Collège de France, Physique Corpusculaire et Cosmologie, IN2P3-CNRS, 11 pl. M. Berthelot, 75231 Paris Cedex, France
[5] Institut d'Astrophysique de Paris, INSU-CNRS, 98 bis Boulevard Arago, 75014 Paris, France
[6] Astronomical Observatory, Copenhagen University, Juliane Maries Vej 30, 2100 Copenhagen, Denmark
[7] Universidad de la Serena, Facultad de Ciencias, Departamento de Fisica, Casilla 554, La Serena, Chile
[8] Departments of Astronomy and Physics, Ohio State University, Columbus, OH 43210, USA
[9] DASGAL, 77 avenue de l'Observatoire, 75014 Paris, France

Received 9 March 2000 / Accepted 15 June 2000

Abstract. We present the EROS nearby supernova ($z \sim 0.02$–0.2) search and the analysis of the first year of data (1997). A total of 80 square degrees were surveyed. Eight supernovæ were detected, four of which were spectroscopically identified as type Ia supernovæ. The search efficiency was determined with a Monte-Carlo simulation taking into account the efficiencies for both supernova detection and host galaxy identification. Assuming that for a given galaxy the supernova rate is proportional to the galactic luminosity, we compute a type Ia supernova explosion rate of: $\mathcal{R} = 0.44^{+0.35\ +0.13}_{-0.21\ -0.07}\, h^2\, /10^{10}\ \mathrm{L}_{\odot B}/\,100\,\mathrm{yrs}$ at an average redshift of ~ 0.1 where the errors are respectively statistical and systematic (type misidentification included).

Key words: surveys – stars: statistics – stars: supernovae: general – cosmology: observations – cosmology: distance scale

1. Introduction

Type Ia supernovæ have been shown to be powerful cosmological distance indicators useful for the determination of the expansion rate H_0 and the density parameters for matter and vacuum energy Ω_M and Ω_Λ (Riess et al. 1998; Perlmutter et al. 1999). As such, they are the subject of intense study and a number of nearby and distant supernova searches have been launched. Studies of type Ia light-curve shapes, peak magnitudes, colors and spectra have been performed in order to get better insight into the nature of these exploding stars.

Supernova rates, and in particular their evolution as a function of redshift, is another probe provided by supernova science. Not only are these rates important for tracking the chemical evolution of the universe, but as a tracer of stellar evolution, they also contain information on which type of progenitor system produces type Ia supernovæ. If the evolution of the supernova rate is understood, they may also be used to determine the cosmological parameters Ω_M and Ω_Λ via the number count-redshift relationship. With enough statistics, it is possible to measure the supernova luminosity function which is of critical importance for understanding Malmquist bias.

The supernova rate has been measured at low redshift in searches based on visual scanning of photographic plates (Cappellaro et al. 1997). At high redshift the rate has been measured with automatic subtraction of CCD images (Pain et al. 1996). The supernova rate for nearby galaxies has previously been estimated using CCD data by Muller et al. (1992). Here we report the first measurement of the rate for low redshift galaxies using CCDs and with a full numerical calculation of the detection efficiency. The search was performed by EROS (Expérience de Recherche d'Objets Sombres).

In 1990 EROS engaged in a search for massive compact halo objects (MACHOs) via gravitational microlensing. Since 1996 EROS has been using a dedicated 1 meter telescope, the Marly telescope, at the ESO La Silla observatory. The telescope is equipped with two detector mosaics, each consisting of eight 2048×2048 pixel CCDs covering a $0.7 \times 1.4\ \mathrm{deg}^2$ field. A

Send offprint requests to: D. Hardin (hardin@in2p3.fr)

⋆ This work is based on observations made at the European Southern Observatory, La Silla, Chile.

⋆⋆ Now at LPNHE, Université Paris VI, 4 place Jussieu, F-75252 Paris Cedex 05, France

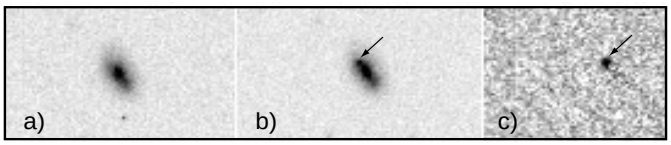

Fig. 1a–c. Illustration of the detection technique (detection images of SN 1997eb). **a** Reference image taken on October 7, 1997. **b** Detection image taken on November 7, 1997. The supernova can barely be distinguished from the galaxy nucleus. **c** The subtracted frame, obtained after geometric and photometric alignment of **a** and **b** frames. The stellar PSFs are matched by convolving the best image. The supernova now stands alone.

dichroic cube allows the simultaneous recording of two images in wide ($\Delta\lambda \sim 200$ nm) non-standard red ($\bar{\lambda} \sim 760$ nm) and visible ($\bar{\lambda} \sim 560$ nm) bands hereafter referred to as $R_{\rm Eros}$ and $V_{\rm Eros}$. The telescope, camera and telescope operation are described in Bauer et al. (1997).

The greater part of EROS observing time is devoted to the search for microlensing events by observing the Magellanic Clouds, the Galactic Bulge and the Galactic Disk (see *e.g.* Palanque-Delabrouille et al. 1998; Derue et al. 1999). However, EROS also devotes 10% of its observing time to the observation of fields at high Galactic latitudes in order to search for supernovæ at low redshifts and to measure stellar proper motions.

The EROS supernova search aims at discovering a homogeneous sample of supernovæ in the low redshift range. Our main scientific goals are the derivation of the nearby supernova rates, and the study of the empirical correlation of the peak luminosity with the light-curve shape. EROS has discovered more than 60 supernovæ since 1997.

In this paper, we present a measurement of the type Ia supernova explosion rate. Because of backgrounds due to variable stars and asteroids, we restricted the search to identified galaxies. To derive a total supernova rate, we therefore assume that the rate for a given galaxy is proportional to the galactic luminosity. For this low statistic supernova sample, no attempt is made to derive rates for different galaxy types.

In Sect. 2, we give the details of our supernova search that are relevant for the rate determination. In Sect. 3 we present the subset of data considered in this analysis and the supernovæ we found. The galaxy sample for the supernova search is described in Sect. 4. In Sect. 5 we describe the determination of our detection efficiency using a Monte Carlo simulation and derive the supernova rate. Finally, in Sect. 6 we present a discussion and interpretation of our results. More details on this measurement can be found in Hardin (1998).

2. The search technique

We searched for supernovæ by comparing an image of a given field with a reference image of the same field taken at least two weeks before. The images are taken during dark time. Only the visible band images are used for the search, but we use both bands when computing the absolute calibration of the images. The technique is illustrated in Fig. 1. Each observation consists of two five minute exposures which are combined to form a ten minute exposure after identification of cosmic rays. Five to ten fields were observed each night. For the observations used in this paper, calibration fields (Landolt 1992) were also observed before and after the series of supernova fields. This allowed us to calibrate our non-standard filters and to eliminate non-photometric nights from the rate measurement.

The automated processing permits the remote analysis in France on computers set up at the La Silla observatory of up to 20 deg^2 during the day following the night of observation. Since the processing is monitored from France, it requires robustness and a limited volume of output.

The method for comparing the reference and the search images is as follows. The reference image is aligned geometrically and photometrically with the search image, and the image of superior seeing is convolved to match the point spread function (PSF) of the other image. The two images are then subtracted and the frame thus obtained is searched for star-like sources. The selection of the candidate supernovæ is performed by applying a set of cuts on the objects detected on the subtracted frame. These cuts are tuned with a Monte-Carlo simulation.

The first and most important cut is applied on the total flux of the candidate, and is equivalent to a limiting magnitude of $V_J \sim 21.5$. Afterwards, a series of cuts involving the comparison of the candidate shape (*i.e.* the second moments of a Gaussian fit) with that of the frame stars is designed to eliminate inaccurate subtractions. Finally, the detection threshold is set slightly higher within 1.8 arcsec of the center of bright galaxies.

The treatment ends with the visual scanning of ~ 5 candidates per square degree by two independent observers. Most of the candidates are residual cosmic rays, subtraction artifacts, asteroids, and variable stars. The residual cosmic rays are identified by the fact that they only appear on one of the two five minute exposures. Asteroids and variable stars are eliminated by requiring the candidate to appear in or near a host identified as a galaxy. As a consequence of this last requirement, no supernovæ with an undetected host can be found. This is taken into account in the calculation of the search efficiency.

3. The data set

For this analysis, we have used the data obtained during the two search runs conducted during October and November 1997. A description of the observed fields is given in Table 1. They have been divided into 3 zones. The southern hemisphere fields have been chosen far from the Galactic plane (mean Galactic latitude $\langle b \rangle \sim -70°$), in a region covered by The Las Campanas Redshift Survey (LCRS, Shectman et al. 1996). While the Abell Cluster fields[1] are centered on Abell Clusters at a mean redshift of $z \sim 0.17$, the search in these fields was not restricted to the galaxies that belong to these clusters. The northern hemisphere fields have been chosen so as to be observable from the La Silla (Chile) and Apache Point (New Mexico, USA) observatories at

[1] Our original program included a study of the peculiar velocities of these clusters (Reiss et al., 1998).

Table 1. List of the surveyed sky zones during the October and the November 1997 runs. The number of fields surveyed in each zone is given in column 2. Due to a temporary malfunction of CCD # 7 on the camera corresponding to the visible band, one field only covers 0.871 deg^2. The total surveyed area is thus ~ 45 (resp. ~ 35) square degrees for the October (resp. November) 1997 run. The southern hemisphere fields are included in the Las Campanas Redshift Survey fields.

zone	# fields	α (J2000)	δ (J2000)	l	b
		October 1997 run			
Southern hem.	43	$22h30' \lesssim \alpha \lesssim 2h30'$	$\delta \sim -40°$	$250° \lesssim l \lesssim 360°$	$-75° \lesssim b \lesssim -60°$
Abell Cluster	8	$2h00' \lesssim \alpha \lesssim 3h00'$	$\delta \sim 0°$	$150° \lesssim l \lesssim 180°$	$-50° \lesssim b \lesssim -60°$
		November 1997 run			
Abell Cluster	4	$2h00' \lesssim \alpha \lesssim 3h00'$	$\delta \sim 0°$	$150° \lesssim l \lesssim 180°$	$-50° \lesssim b \lesssim -60°$
Northern hem.	36	$3h00' \lesssim \alpha \lesssim 4h00'$	$\delta \sim 0°$	$175° \lesssim l \lesssim 190°$	$-35° \lesssim b \lesssim -55°$

Table 2. Main characteristics of the supernovæ detected during the October and the November 1997 runs. In the third column, (l.c.) indicates that the supernova type was derived from its light curve. All magnitudes are corrected for Galactic absorption. Note that SN 1997dk and SN 1997dl occurred in the same galaxy, 2 months apart according to their spectra. The references are as follows: (1) IAU6760, 1997; (2) IAU6762, 1997; (3) IAU6782, 1997, and IAU6785, 1997.

IAU name		date	type	z	host R_c mag.	discovery V_J mag	dist. from host core
SN 1997dh	(1)	20/10/1997	Ic	0.05	15.7	20.	5.0 ”
SN 1997dk	(2)	26/10/1997	Ia	0.05	15.2	20.	11.0 ”
SN 1997dl	(2)	26/10/1997	Ia	0.05	15.2	19.5	11.0 ”
SN 1997dm	(2)	26/10/1997	IIp (l.c.)	0.03	14.4	21.	6.7 ”
SN 1997eb	(3)	19/11/1997	II (l.c.)	0.08	17.1	21.5	2.9 ”
SN 1997ec	(3)	20/11/1997	IIp (l.c.)	0.12	16.3	21.5	3.7 ”
SN 1997ed	(3)	22/11/1997	Ia	0.15	17.5	21.	2.8 ”
SN 1997ee	(3)	23/11/1997	Ia	0.17	17.0	21.	8.6 ”

the time of the November 1997 run. As a consequence, their mean Galactic latitude ($\langle b \rangle \sim -50°$) is not as high as in the southern hemisphere zone. The total area of sky (80 square degrees) was covered over a period of 10 days.

Among the 8 detected supernovæ, 5 could be classified according to their spectra. The type of the three remaining supernovæ was obtained using the shapes of their light curves. The characteristics of these eight supernovæ are summarized in Table 2.

4. The galaxy sample

In order to determine the supernova rate, we must have a well-defined sample of potential host galaxies with a known distribution of redshifts. In this section, we describe our galaxy identification and redshift determination algorithms and their verification using LCRS galaxies in our fields.

4.1. Galaxy identification

The position and flux of the sources on the reference and detection frames are measured with the software for source extraction SExtractor (Bertin & Arnouts 1996). SExtractor measures the total flux of extended sources, and provides in addition a star-galaxy separation estimator, CLASS STAR, which uses the intensity profile.

Our galaxy selection criterion is based on the (total) $V_{\rm Eros}$ magnitude and CLASS STAR. Because of the PSF variation over the CCD mosaic, the cut applied on CLASS STAR differs from one CCD to the other. On the other hand, the cut on $V_{\rm Eros}$ is set equal for all frames and corresponds to a magnitude $R_{c0} \sim 18.7$ for the October 1997 search fields, and $R_{c0} \sim 18.4$ for the November 1997 search fields. This difference is due to Galactic absorption. The cut on the galaxy magnitude was to ensure that the host was classified as such during the visual scanning. At $z = 0.1$, this corresponds to an absolute magnitude of $M_{R_c} \sim -20. + 5\log(H_0/60\,{\rm kms}^{-1}{\rm Mpc}^{-1})$ for the host galaxy.

This selection criterion was first tested on the fields shared with the LCRS: 90% of the LCRS redshift catalog galaxies were identified as such by our criterion, and 95% of the selected objects with a magnitude $R_c \lesssim 17.5$ (LCRS completeness limit) were LCRS galaxies.

Having identified the galaxies on our frames and derived their R_c (total) magnitude from their $V_{\rm Eros}$ and $R_{\rm Eros}$ magnitudes and the calibration (see Sect. 2), we obtain a galaxy count per magnitude and per deg^2, which we can compare with published counts. The agreement is illustrated in Fig. 2. One can also identify the complementary set of objects as stars and obtain in this way star counts as a function of magnitude. These star counts compare well with the Galactic star-count model of Bahcall & Soneira (1984).

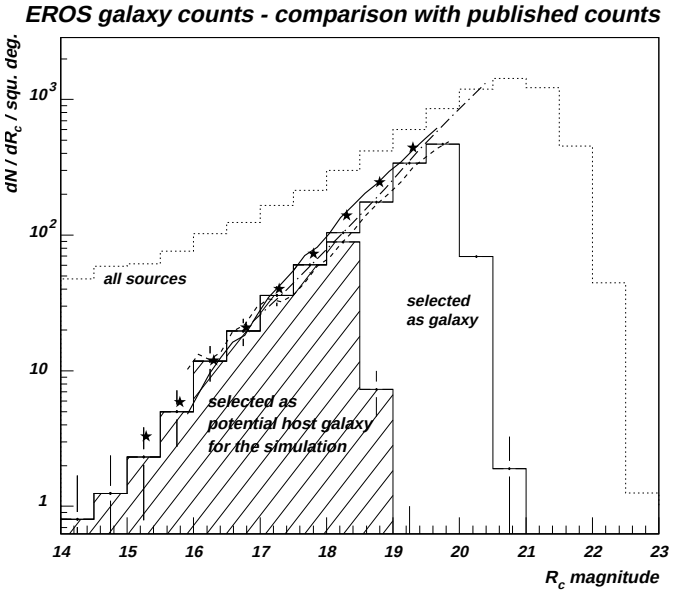

Fig. 2. Comparison of EROS galaxy counts (histograms) with counts from Bertin & Dennefeld (1997; stars), Weir et al. (1995; bold dash-dot line), and the northern (bold full line) and southern counts (bold dashed line) from Picard (1991). The dotted line histogram shows all the detected sources on the frames, both stars and galaxies, the full line histogram the objects selected as galaxies (with $R_c \lesssim 20.2$), and the hatched histogram the objects selected as potential hosts for the simulation, *i.e.* with a magnitude $R_c \lesssim 18.7$. This corresponds to a solid angle of 38 deg^2 (October 1997 data). There is good agreement between our galaxy counts and published counts.

At this stage, ~ 225 objects per deg^2 are selected as potential host galaxies.

4.2. Magnitude-redshift relationship

For a galaxy of a given magnitude $R_{\rm c\,gal}$, the probability that its redshift is z is given by:

$$p(z|R_{\rm c\,gal}) \propto \frac{dV_c}{dz}(z) \times \frac{dN_{\rm gal}}{dM}\,(M = R_{\rm c\,gal} - \mu_L(z) - K_{\rm gal}(z)) \quad (1)$$

In this equation, dV_c/dz is the derivative of the comoving volume with respect to z, and μ_L is the luminosity distance modulus. The cosmological parameters $(\Omega_M; \Omega_\Lambda)$ are set to the value $(0.3; 0.)$. Taking the values $(\Omega_M; \Omega_\Lambda) = (0.3; 0.7)$ based on distant type Ia supernovæ (Riess et al. 1998; Perlmutter et al. 1999) decreases the computed rate by less than 5%.

The distribution of the number of galaxies per unit absolute magnitude $dN_{\rm gal}/dM$ is the Schechter law:

$$\frac{dN_{\rm gal}}{dM} \propto 10^{-0.4\times(\alpha+1)\times(M-M_*)} \exp\left(-10^{-0.4\times(M-M_*)}\right) \quad (2)$$

measured by the LCRS (Lin et al. 1996) where $\alpha_{\rm LCRS} = -0.7$ and $M_{*\,R_c\,\rm LCRS} = -20.29 + 5\log h$ ($h = H_0/100\,{\rm kms}^{-1}{\rm Mpc}^{-1}$).

The K-correction is simply given by $K_{\rm gal}(z) = 2.5\log(1+z)$ as proposed by Lin et al. (1996).

For a galaxy magnitude of $R_{\rm c\,gal} \simeq 17$, the mean and rms value of the z-distribution thus obtained are respectively ~ 0.1 and ~ 0.05.

The model was checked by comparing, for each galaxy with an LCRS redshift, the mean of $p(z|R_{\rm c\,gal})$ with the measured LCRS redshift. Satisfactory agreement was obtained after adding 0.25 to the EROS total magnitudes (as measured with SExtractor) so as to align them with the isophotal LCRS magnitudes.

5. The detection efficiency and the supernova rate

The supernova rate $\mathcal{R}$ in the rest frame is expressed in SNu, *i.e.* in supernovæ per unit time per unit blue luminosity, $1\,{\rm SNu} = 1\,{\rm SN}\,/10^{10}\,{\rm L}_{\odot B}/\,100\,{\rm yrs}$. The number of supernovæ $\mathcal{N}$ expected to be detected is given by a sum over the observed galaxies i weighted by their blue luminosities L_i:

$$\mathcal{N} = \mathcal{R} \times \mathcal{S}, \quad (3)$$
$$\mathcal{S} = \sum_{\rm gal.\ i} L_i \int_{-\infty}^{\infty} \epsilon_i(t, z_i)\, dt$$

where $\epsilon_i(t, z_i)$ is the efficiency to detect in galaxy i a type Ia supernova whose maximum occurs at time t in the supernova rest frame. The efficiency clearly depends on the galaxy redshift z_i but also on other factors such as the galactic luminosity and surface-brightness profile. The integral $\int \epsilon_i dt$ is sometimes called the "control time" for the galaxy i.

We now need to determine the sum $\mathcal{S}$ so the rate can be evaluated through Eq. 3. We do not know the luminosities of most of the observed galaxies because most of their redshifts are not known. As discussed in the previous section, we do, however, know the probability $p(z|R_{\rm c\,gal})$ that the galaxy of magnitude $R_{\rm c\,gal}$ has a redshift z. We therefore replace the above expression for $\mathcal{S}$ with

$$\mathcal{S} = \sum_{\rm gal.\ i} \int_0^{\infty} dz\; p(z|R_{c\,i})\, L_i(R_{c\,i}, z) \int_{-\infty}^{\infty} \epsilon_i(t, z)\, dt \quad (4)$$

where the blue luminosity L_i is computed using the magnitude $R_{c\,i}$ and the redshift z. The double integral in this equation was evaluated for each galaxy by Monte Carlo simulation of supernovæ that are subjected to the same detection procedures as the real data.

Because there is a better match between the EROS visible band and the standard V filter than with the standard B filter, the absolute luminosities of galaxies are first computed in the standard V band, and then converted into absolute luminosities in the standard B band. We use the difference between the solar $\langle B-V\rangle$ colour: $\langle B-V\rangle_\odot = 0.65$ and a mean $\langle B-V\rangle$ colour for galaxies, computed from the results of Fioc & Rocca-Volmerange (1997): $\langle B-V\rangle_{\rm gal} = 0.77$.

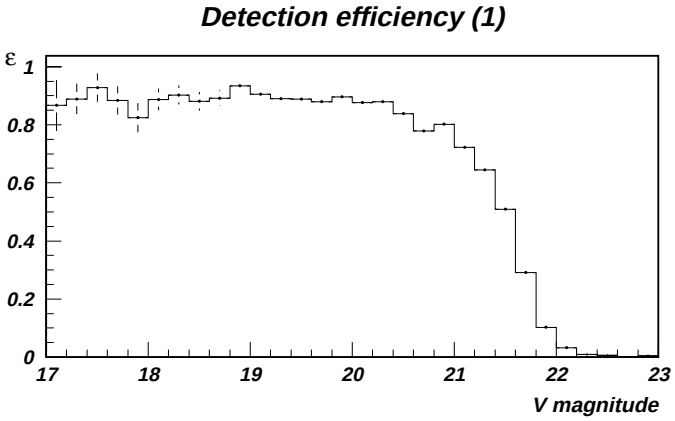

Fig. 3. The detection efficiency ε as a function of the simulated supernova magnitude V_J at discovery. It corresponds to a limiting magnitude $V_J \sim 21.5$. The maximum efficiency is below 1 because of the masked areas near CCD defects and saturated stars.

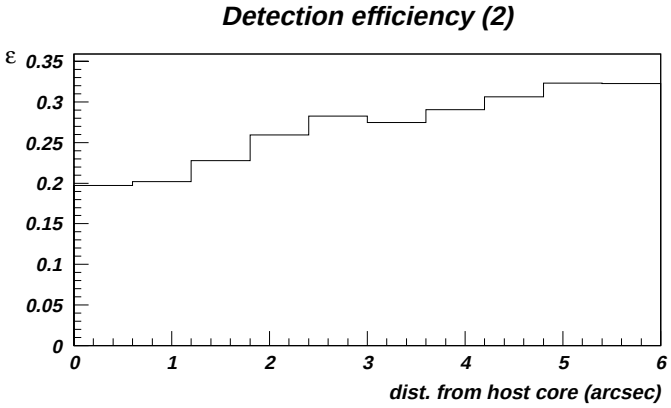

Fig. 4. Dependence of the detection efficiency ε on the distance between the simulated supernova and its host galaxy core. The average efficiency is as low as ∼30% because supernova light curves are sampled up to 120 days after maximum, causing $\sim 75\%$ of them to drop below $V_J = 22$.

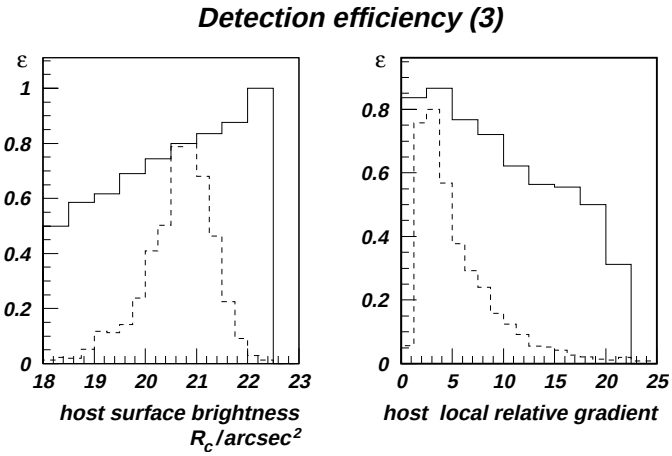

Fig. 5. Detection efficiency ε as a function of the host galaxy surface brightness (left pannel) and of the local gradient at the point where the simulated supernova is added (right pannel). The local gradient was taken to be $g = \max\left(\mathrm{pixel}(x_i, y_i) - \mathrm{pixel}(x_j, y_j)\right)_{|j-i|\leq 1} / B$ where B is the local Poisson noise. The distributions of the surface brightness and the local gradient are superimposed (dashed lines). The distributions are shown for supernovæ whose magnitude is in the range $20.5 < V_J < 21$.

5.1. Supernova simulation

The Monte Carlo simulation proceeds as follows. For each potential host galaxy, a series of redshifts is drawn randomly according to the distribution appropriate for the galaxy apparent magnitude. For each redshift, a time t since maximum is drawn uniformly between -15 and $+120$ days in the supernova rest frame. The absolute magnitudes M_{V_J} and M_{R_c} of the supernova at that time are taken from the templates in these standard filters provided by Riess et al. (1996). To account for the observed spread of supernova luminosities, a gaussian scatter $\Delta M = 0.2\,\mathrm{mag}$ was added. The apparent magnitude of the simulated supernova is computed from the redshift using the K-correction from Nugent & Kim (in preparation) and assuming $(\Omega_M, \Omega_\Lambda) = (0.3, 0.)$ as above.

The supernova standard apparent magnitudes are then converted into a V_{Eros} flux using our calibration. The position of the supernova in the host galaxy is drawn according to a two-dimensional Gaussian distribution, the first and second order moments and orientation of which are those of the host object.

As supernovæ are stellar sources, they appear on the frame with the same PSF as the field stars do. The PSF is modeled by a two-dimension integrated Gaussian. Its second order moments are set to the mean moments computed by fitting the stars on the same CCD quadrant, in order to take into account the spatial variation of the PSF.

5.2. Detection efficiency

The detection efficiency is derived by comparing the list of simulated supernovæ and the list of the supernovæ selected by the search cuts.

The detection efficiency as a function of magnitude is shown in Fig. 3. It appears as a smoothed step function, corresponding to a limiting magnitude $V_J \sim 21.5$. There is a slight dependence on the distance of the supernova from the host galaxy core, as shown in Fig. 4.

As foreseen, the detection efficiency depends on the host galaxy characteristics, such as the surface brightness or the local gradient where the simulated supernova is added. These results are presented in Fig. 5, where the distribution of these two parameters have been superimposed on the efficiency. The distributions are shown for supernovæ whose magnitude is in the range $20.5 < V_J < 21$. They peak where the efficiency is good, thus moderating the impact of the efficiency behaviour.

5.3. Redshift distribution

The Monte-Carlo computed redshift distribution of detected supernovæ is shown in Fig. 6. The thin solid line shows the distribution when all the analysis cuts are applied. For comparison, the dotted line shows the redshift distribution when

only two cuts are applied, one on the supernova magnitude $V_J < V_{J_0} = 21.5$, and one on the host galaxy $V_{\rm Eros}$ magnitude equivalent to $R_{c\,\rm gal} < R_{c\,\rm gal_0} = 18.7$. The thick solid line shows the distribution obtained with an analytic model where we assume that the type Ia supernova rate is proportionnal to the host galaxy luminosity and that the galaxy luminosity distribution is given by the LCRS Schechter law (Eq. 2). In this analytic model the cuts are described by two step-functions whose thresholds are respectively V_{J_0} and $R_{c\,\rm gal_0}$. Using this analytic model, we find that imposing the host galaxy magnitude cut reduces the number of detected supernova by a factor ~ 2.3.

The observed redshift distribution of the 4 discovered type Ia supernovæ is in agreement with the Monte-Carlo distribution (the Kolmogorov-Smirnov compatibility test gives a 25% probability), although the small-number statistics prevents any definitive conclusion. The mean and rms of the expected redshifts, respectively 0.14 and 0.06, are to be compared with the mean and rms of the observed redshifts, respectively 0.10 and 0.06.

5.4. Explosion rate

The rate is computed by dividing the number of observed supernovæ $\mathcal{N}_{\rm obs}$ by the sum $\mathcal{S}$:

$$\mathcal{R} = \mathcal{N}_{\rm obs}/\mathcal{S} \tag{5}$$

The sum obtained is $\mathcal{S} = 9.09\,10^{12}\,h^{-2}\,{\rm L}_{\odot B}\,{\rm yr}$. For $\mathcal{N}_{\rm obs} = 4$ type Ia supernovæ, this corresponds to a rate $\mathcal{R} = 0.44^{+0.35}_{-0.21}\,h^2\,/10^{10}\,{\rm L}_{\odot B}/\,100\,{\rm yr}$ where the error is statistical and given at a 68% confidence level.

6. Discussion

The numerical calculation of the efficiency makes it possible to study various systematic effects. We study here the effects inherent in the hypotheses used in the Monte Carlo simulation, such as the calibration relations or the assumed type Ia supernova light-curve shape.

6.1. Calibration

The calibration enters the calculation at three different steps: when measuring the galaxy magnitude R_c, which is used to draw its redshift, when computing the ADU flux of a simulated supernova as a function of its V_J and R_c magnitudes, and when estimating the galaxy absolute luminosity in the V_J filter for the rate computation in SNu. The redshift galaxy distribution is verified with the LCRS galaxies, therefore we shall only take into account here the last two steps. Their contributions are of opposite sign, so that the estimated 10% uncertainty in the calibration zero-point yields only a 5% uncertainty in the computed rate.

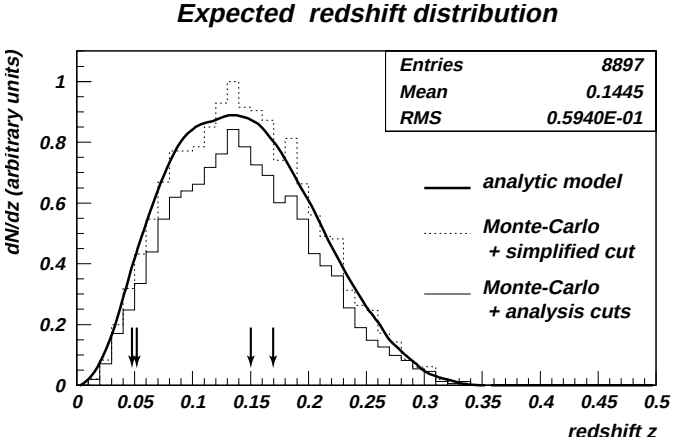

Fig. 6. The expected redshift distribution. The thin solid line shows the distribution in z derived from the Monte-Carlo simulation when the analysis cuts are applied. The dotted line shows the same but with only two cuts applied, one on the supernova magnitude ($V_J < 21.5$) and the other one on the host galaxy $V_{\rm Eros}$ magnitude equivalent to $R_{c\,\rm gal} \lesssim 18.5$. The latter distribution compares well with a simple analytic model as described in the text (thick solid line). The arrows indicate the redshift values of the 4 discovered type Ia supernovæ.

6.2. Galaxy counts and redshift distribution

To take into account the requirement for the detected supernova to be found in a galaxy, potential host galaxies were selected by requiring that their magnitude R_c satisfy $R_c < R_{c0}$ (Sect. 4.1). A 0.2 magnitude shift on R_{c0} translates into a 10% shift on the rate.

The galaxy sample misidentification is estimated to be about 10% (Sect. 4.1), which gives rise to a 10% uncertainty in the computed rate.

6.3. Supernova luminosity distribution

In the simulation, the supernova light curve was approximated by V_J and R_c templates of Riess et al. (1996). The light-curve shape is described through two parameters: the peak magnitude $M_{V_J\,\rm max}$ and the stretch factor s (Perlmutter et al. 1999). We assumed in the analysis that $M_{V_J\,\rm max} = -18.4 + 5\log h$ with an added gaussian scatter of 0.2 mag, which corresponds to the observed distribution for the 16 supernovæ from the Hamuy et al. (**?**) sample reanalysed in Perlmutter et al. (1999). No stretch factor correction was taken into account, *i.e.* s was set to $s = 1$. To test the robustness of this analysis, we reperformed the analysis assuming, following Perlmutter et al. (1999), that the peak magnitude is described by $M_{V_J\,\rm max} = M_{V_{J_0}\,\rm max} - 0.6 \times (s-1)$, where the $M_{V_{J_0}\,\rm max}$ distribution is a Gaussian centered on $M_{V_J} = -18.4 + 5\log h$ with a scatter $\sigma = 0.2$ mag., and s is a Gaussian centered on $s = 1$ with a scatter $\sigma = 0.1$. The rate calculated with these assumptions differed from that calculated with the standard assumptions by less than 1%.

On the other hand, it seems possible that the type Ia supernova mean peak magnitude might be uncertain to about 0.1

Table 3. Summary of systematic errors.

Magnitude calibration	$\pm$ 5%
Limiting magnitude R_{c0} for the galaxy selection	$\pm$10%
Galaxy misidentification	$\pm$10%
SN mean peak magnitude	$\pm$ 5%
SN type misidentification	$^{+25}_{-\ 0}$%
Total systematic error	$^{+30}_{-16}$%

mag. A shift of 0.1 mag in the peak magnitude results in a 5% variation of the rate.

6.4. Total number of detected type Ia

The type of SN 1997eb is unclear. This is taken into account by adding $^{+0.11}_{-0.00}$ SNu to the systematic uncertainty.

7. Conclusion

We measure a rate of:

$$\mathcal{R} = 0.44^{+0.35\ +0.13}_{-0.21\ -0.07}\, h^2 \text{ SNu}$$

where the systematic errors from Table 3 have been added in quadrature. The statistical error corresponds to a 68% confidence level. This rate compares well with the rate derived by Cappellaro et al. (1999) from the combined sample of five nearby photographic searches, $\mathcal{R} = 0.35 \pm 0.11\, h^2$ SNu at a mean redshift of $z \sim 0.01$. Similarly, our rate compares well with the Supernova Cosmology Project rate for type Ia at $z \sim 0.4$ derived by Pain et al. (1996), $\mathcal{R} = 0.82^{+0.65}_{-0.45}\, h^2$ SNu.

The rate can also be expressed in $h^3/\mathrm{Mpc}^3/\mathrm{yr}$ by multiplying the rate in SNu by the luminous density of the universe $\rho_L = 1.4 \pm 0.1\, 10^8\, h\ \mathrm{L}_\odot\, \mathrm{Mpc}^{-3}$ (Lin et al. 1996). This gives:

$$\mathcal{R} = 0.62 \pm ^{+0.49+0.19}_{-0.29-0.11}\, 10^{-4}\, h^3/\mathrm{Mpc}^3/\mathrm{yr}.$$

Acknowledgements. We are grateful to D. Lacroix and the technical staff at the Observatoire de Haute Provence and to A. Baranne for their help in refurbishing the MARLY telescope and remounting it in La Silla. We are also grateful for the support given to our project by the technical staff at ESO, La Silla. We thank J.F. Lecointe for assistance with the online computing. We also thank S. Deutsua, R. McMillan, H. Newberg, P. Nugent, C. Pennypacker, S. Perlmutter and M. Strauss for providing spectra of SN 1997eb, SN 1997ec, SN 1997ed and SN 1997ee. We are grateful to R. Pain for helpful discussions. We also thank the referee for his helpful remarks.

References

Bahcall J. N., Soneira R., 1984, A&AS, 55, 67.
Bauer F., de Kat J., Afonso C., et al. (EROS collaboration), 1997, in Proceedings of the "Optical Detectors for Astronomy" workshop (ESO, Garching)
Bertin E., Arnouts S., 1996, A&AS, 117, 393.
Bertin E., Dennefeld M., 1997, A&A, 317, 43.
Cappellaro E., Evans R., Turatto M., et al., 1999, A&A, 351, 459.
Cappellaro E., Turatto M., Tsvetkov D.Yu., et al., 1997, A&A, 322, 431.
Derue F., Afonso C., Alard C., et al., 1999, A&A, 351, 87.
Fioc M., Rocca-Volmerange B., 1997, A&A, 326, 950.
Hardin D., 1998, PhD thesis in French, Université de Paris 11, DAPNIA-SPP 98-1002.
IAU circular 6760, 1997, the EROS collaboration.
IAU circular 6762, 1997, the EROS collaboration.
IAU circular 6782, 1997, the EROS collaboration.
IAU circular 6785, 1997, Deustua S., McMillan R., Newberg H.J.M. et al.
Landolt A.U., 1992, AJ, 104, 340.
Lin H., Kirshner R.P., Shectman S.A., et al., 1996, ApJ, 464, 60.
Muller R.A., Newberg H.J.M., Pennypacker C.R., et al., 1992, ApJ, 384, L9.
Nugent P., Kim A., in preparation.
Pain R., Hook I.M., Deustua S., et al., 1996, 473, 356.
Palanque-Delabrouille N., Afonso C., Albert J.-N., et al., 1998, A&A, 332, 1.
Perlmutter S., Aldering G., Goldhaber G., et al., 1999, ApJ, 517, 565.
Phillips M.M., 1993, ApJ, 413, L105.
Picard A., 1991, AJ 102, 445.
Reiss D.J., Germany L.M., Schmidt B.P., et al., 1998, AJ, 115, 26.
Riess A.G., Press W.H., Kirshner R.P., 1996, ApJ, 473, 88.
Riess A.G., Filippenko A.V., Challis P., 1998, AJ, 116, 1009.
Shectman S.A., Landy S.D., Oemler A., et al., 1996, ApJ 470, 172.
Weir N., Djorgovski S., Fayyad U.M., 1995, AJ 110, 1.